

LOCATING THE “MISSING” BARYONS WITH EXTRAGALACTIC DISPERSION MEASURE ESTIMATES

MATTHEW MCQUINN¹
Draft version April 19, 2019

ABSTRACT

Recently, Thornton and coworkers (2013) confirmed a class of millisecond radio bursts likely of extragalactic origin that is well-suited for estimating dispersion measures (DMs). We calculate the probability distribution of $DM(z)$ in different models for how the cosmic baryons are distributed (both analytically and with cosmological simulations). We show that the distribution of DM is quite sensitive to whether the “missing” baryons lie around the virial radius of $10^{11} - 10^{13} M_{\odot}$ halos or further out, which is not easily constrained with other observational techniques. The intrinsic contribution to DM from each source could complicate studies of the extragalactic contribution. This difficulty is avoided by stacking based on the impact parameter to foreground galaxies. We show that a stacking analysis using a sample of ~ 100 DM measurements from arcminute-localized, $z \gtrsim 0.5$ sources would place interesting constraints at $0.2 - 2$ halo virial radii on the baryonic mass profile surrounding different galaxy types. Conveniently for intergalactic studies, sightlines that intersect intervening galactic disks should be easily identified owing to scattering. A detectable level of scattering may also result from turbulence in the circumgalactic medium.

Subject headings: cosmology: theory — large-scale structure of universe — intergalactic medium — radio continuum: general

1. INTRODUCTION

Approximately 5% of the cosmic baryons at $z \sim 0$ are observed to lie within galaxies, 5% are seen as X-ray coronae in massive groups and clusters, and 30% reside in a warm intergalactic phase observed in Ly α absorption (Kauffmann et al. 2003; Fukugita & Peebles 2004; Penton et al. 2004). The constraints on the locations of the rest (the majority) of the cosmic baryons are weaker, as they reside at densities and temperatures that do not afford significant absorption or emission, except sometimes from highly-ionized states of oxygen (Cen & Ostriker 1999; Bregman 2007; Shull et al. 2012).

Finding these “missing” baryons would inform models for accretion onto, and feedback within, galactic halos. Half of the Universe’s dark matter resides in halos with $m_h > 10^{10} M_{\odot}$, where m_h is the halo mass. However, much less than half of the baryons are observed to lie within these halos: The $z = 0$ stellar mass to halo mass ratio for $m_h = 10^{12} M_{\odot}$ has been estimated to be $0.2^{+0.2}_{-0.1} f_b$ (Behroozi et al. 2013), where $f_b = \Omega_b/\Omega_m$, declining sharply towards both lower and higher masses. The diffuse galactic gas mass to halo mass ratio is even a few times smaller. Much of $f_b m_h$ has been observed as hot intrahalo gas in $m_h \gtrsim 10^{14} M_{\odot}$ halos (Dai et al. 2010). However, for $m_h \lesssim 10^{13} M_{\odot}$, the bulk of the unseen baryons cannot constitute a hot atmosphere, as it would be thermally unstable (Sharma et al. 2012). Most of the baryons associated with these lower mass halos likely lie outside of the virial radius.

Here we consider whether the dispersion measures (DMs) of extragalactic sources could aid this cosmic census. In contrast to the other observables, every diffuse ionized baryon along a sightline contributes equally to the DM. Prior to recent developments, there was no reason to believe that redshifted sources existed

for which DM could be measured. First, a class of out-of-the-plane, highly dispersed (and hence likely extragalactic) millisecond radio bursts was identified in Thornton et al. (2013), confirming previous indications (Lorimer et al. 2007). The four bursts reported in Thornton et al. (2013) have redshifts of $0.5 - 1$ if their DM were sourced by the intergalactic medium (IGM). Lorimer et al. (2013) forecast that widefield radio interferometers that are presently coming online could detect tens per day of these events. In a second development, Lieu & Duan (2013) and Lovelace & Richards (2013) argued that DM could be measured even for *non-variable* extragalactic synchrotron sources.

Previous theoretical investigations of the uses of extragalactic DM measurements assumed a homogeneous universe (Ioka 2003; Inoue 2004). Here we consider the effects of inhomogeneities, which lead to substantial sightline-to-sightline scatter around the mean $DM(z)$. We show that the statistics of this scatter constrain the locations of the “missing” baryons.

The calculations in this Letter assume a flat Λ CDM cosmological model, consistent with the most recent determinations of Planck Collaboration et al. (2013), and the Sheth & Tormen (2002) halo mass function.

2. SIGHTLINE-TO-SIGHTLINE SCATTER IN DM

Photons propagate through the cosmic plasma at a speed that depends on frequency. The delay between the arrival time of a photon with observed frequency in units of GHz, ν_{GHz} , and one with a much higher frequency is given by

$$\Delta t = 4.2 \nu_{\text{GHz}}^{-2} \left(\frac{\text{DM}}{10^3 \text{ cm}^{-3} \text{ pc}} \right) \text{ s}, \quad (1)$$

¹ Hubble fellow

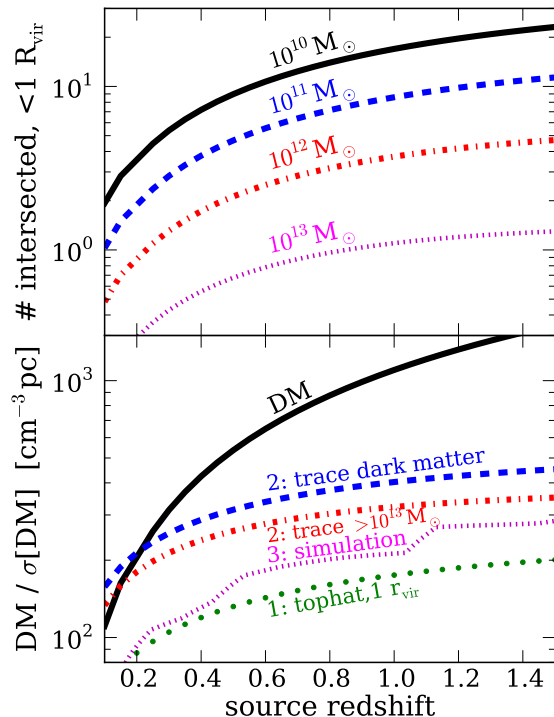


FIG. 1.— Top panel: The average number of halos above the specified mass thresholds that a sightline intersects within $1 r_{\text{vir}}$. Bottom panel: The mean dispersion measure (solid curve) as well as the standard deviation in its value for the considered models (other curves).

where DM is the “dispersion measure.” For cosmological distances,

$$\text{DM}(z_s) = \int_0^{\chi(z_s)} d\chi \frac{\rho_e(z, \hat{n})}{(1+z)^2}, \quad (2)$$

where $d\chi = c dz/H(z)$ is the differential of the conformal distance, χ , $\rho_e(z, \hat{n})$ is the electron number density at redshift z in direction \hat{n} , and z_s is the source redshift. In the bottom panel of Figure 1, the solid curve shows the mean value of DM(z). For this curve and subsequent analytic calculations, we take *all* of the cosmic baryons to be in a diffuse, fully ionized phase.

The sightline-to-sightline scatter in DM(z) primarily owes to scatter in the number of collapsed systems that a sightline encounters. The top panel of Figure 1 shows the number of halos above the specified halo mass thresholds that the average sightline intersects within $1 r_{\text{vir}}$. For a sightline with $z_s = 1$, on average it intersects $N(m_h) = 1, 3, 10$, and 20 halos with m_h greater than $10^{13}, 10^{12}, 10^{11}$, and $10^{10} M_\odot$, respectively. The fraction of the dark matter that resides in halos above these masses is $f = 0.19, 0.30, 0.39$, and 0.46 at $z = 0$ ($f = 0.07, 0.16, 0.26, 0.33$ at $z = 1$). Halos with $m_h < 10^{10} M_\odot$ are below the Jeans’ mass of the IGM and, therefore, unlikely to be overdense in gas.

The sightline-to-sightline variance in DM(z_s) is given

by

$$\begin{aligned} \sigma^2[\text{DM}] &= \int_0^{z_s} \frac{c dz_1}{a_1 H(z_1)} \int_0^{z_s} \frac{c dz_2}{a_2 H(z_2)} \bar{\rho}_e^2(0) \langle \delta_e(z_1) \delta_e(z_2) \rangle, \\ &\approx \int_0^{z_s} \frac{c dz}{H(z)} (1+z)^2 \bar{\rho}_e^2(0) \int \frac{d^2 k_\perp}{(2\pi)^2} P_e(k_\perp, z), \end{aligned}$$

where $a_n = (1+z_n)^{-1}$, $\bar{\rho}_e(z)$ is the mean electron number density, $\delta_e(z)$ is the electron overdensity, $P_e(k, z) = \langle |\tilde{\delta}_e(k, z)|^2 \rangle$ is its spatial 3D power spectrum, tildes denote the Fourier dual in the convention where 2π ’s appear only under dk ’s, and $\langle \dots \rangle$ indicates an ensemble average.

To calculate P_e and hence $\sigma^2[\text{DM}]$, we consider three models (ordered in increasing sophistication) for halos’ gas profile of the ionized baryons:

1. The baryons associated with $m_h > 10^{10} M_\odot$ halos are distributed as a top hat with radius $X r_{\text{vir}}$, which yields for each halo a DM at $R \ll X r_{\text{vir}}$ of

$$\Delta_{\text{DM}} = 28 (1+z) \frac{\alpha^{2/3}}{X^2} \left(\frac{M}{10^{12} M_\odot} \right)^{1/3} \text{ cm}^{-3} \text{ pc}.$$

Here, α is the dark matter density within $1 r_{\text{vir}}$ in units of 200 times its cosmic mean. The unassociated baryons (or those associated with less massive halos) in this model and Model 2 are assumed to trace the linear density field. As long as they are more diffuse than the baryons associated with the more massive halos, this assumption has little impact on our results.

2. The baryons trace the dark matter halo profile above a certain mass threshold, m_* . Our calculations assume NFW halo profiles (Navarro et al. 1996) and the concentration–halo mass relation of Bullock et al. (2001). In addition, we use the case $m_* = 10^{13} M_\odot$ to approximate the Sharma et al. (2012) model for the intrahalo medium. Sharma et al. (2012) find that halos with $m_h > 10^{13} M_\odot$ have the potential to retain most of their gas in a virialized intrahalo medium, whereas lower mass halos cannot as densities would be required that are thermally unstable.²
3. The baryon distribution in the “swinds” $40 h^{-1} \text{ Mpc}$ cosmological simulation of Faucher-Giguère et al. (2011), which was run with the GADGET-3 smooth particle hydrodynamics code (Springel 2005).³ This simulation uses the Springel & Hernquist (2003) galactic wind prescription, with $2 M_\odot$ ejected in a 342 km s^{-1} wind for every $1 M_\odot$ of star formation. These parameters were chosen to match observations of the $z = 0$ stellar mass function.

We use *the standard halo model* to calculate P_e for Models 1 and 2, but with the specified baryonic profiles rather than NFW profiles. *The standard halo model*

² We also investigated more sophisticated implementations of the Sharma et al. (2012) model and found similar results.

³ This simulation consists of 512^3 gas and dark matter particles, with 12 snapshots between $0 < z < 1$. We estimate that the large-scale modes not captured in this simulation’s volume contribute directly $60 \text{ cm}^{-3} \text{ pc}$ to $\sigma[\text{DM}]$ for $z_s = 1$, which should be added in quadrature to the component from within the volume.

approximates correlations in the cosmological density field as a superposition of the linear density field correlations (convolved with the halos' profiles) plus a Poissonian term that results from internal correlations within each halo. This ansatz has met much success reproducing the statistics of the nonlinear dark matter field (see Cooray & Sheth 2002 for a review). For Model 3, we instead trace skewers through the simulation volume on the light cone, using the simulation's nearest temporal snapshot as the realization of the cosmological density field.

The curves in the bottom panel of Figure 1 show our estimates for $\sigma[\text{DM}]$ in the three baryonic profile models. Model 2 with $m_* = 10^{10} M_\odot$, annotated as “trace the dark matter,” results in the largest dispersion, with $\sigma[\text{DM}] = 400 \text{ cm}^{-3} \text{ pc}$ at $z = 1$. The other models have reduced dispersion, with the $1 r_{\text{vir}}$ top hat model having the smallest with $\sigma[\text{DM}] = 180 \text{ cm}^{-3} \text{ pc}$. The dispersion in the case where the baryons trace NFW halos for $m_h > 10^{13} M_\odot$ (which mimics the Sharma et al. 2012 model) is only somewhat smaller than the dark matter tracing case, which we explain in Section 3. These variances are not only a signal, but set the noise of the stacking analysis discussed in Section 4.

Our models have ignored the contribution of a disk electronic component to $\sigma[\text{DM}]$. There are two justifications for this omission. First, the disk component is unlikely to contribute significantly to $\sigma[\text{DM}]$. In the Cordes & Lazio (2002) model for the Milky Way electron distribution, an $r = 18 \text{ kpc}$ thick disk contributes a maximum of $60 \text{ cm}^{-3} \text{ pc}$ for sightlines perpendicular to the disk plane, and the thick disk is the largest contributor to the electronic column everywhere except in the Galactic Center. Consider a toy model motivated by the Milky Way thick disk in which all galactic disks have a column of $\text{DM}_{\text{disk}} = 100 \text{ cm}^{-3} \text{ pc}$. If 10% of $z_s = 1$ sightlines intersect disks (a factor of a few higher than empirical estimates based on damped Ly α systems; Wolfe et al. 2005),⁴ the standard deviation in DM from disks alone would be just $\sigma_{\text{disk}}[\text{DM}] = 30 \text{ cm}^{-3} \text{ pc}$, which roughly adds in quadrature to the extragalactic component of $\sim 200 \text{ cm}^{-3} \text{ pc}$. Second, we show in Section 5 that sightlines that intersect interloping disks similar to or denser than the Milky Way thick disk can be distinguished from other sightlines owing to scattering.

3. PROBABILITY DISTRIBUTION FUNCTION OF DM

The characteristic function of the DM distribution – the Fourier transform of the PDF – can be calculated in a manner that is similar to the derivation in Zhang & Sheth (2007) concerning the cosmological Compton y -parameter. For a source at redshift z_s , the

⁴ We can also estimate the probability to intersect a disk analytically. The isothermal potential model in Mo et al. (1998) yields a disk cross section of $\Sigma_{\text{disk}} = \pi(\lambda r_{\text{vir}})^2/2 \times 2/\pi = 0.0025 r_{\text{vir}}^2$, where the latter is evaluated for a halo spin parameter of $\lambda = 0.05$ (the RMS found in cosmological simulations). This model tends to over predict the stellar scale radius of disks. However, it produces a scale radius that is approximately half of the estimated termination radius of the Milky Way's electronic thick disk. Using the calculations in the top panel of Figure 1, a sightline with $z_s = 1$ intersects the galactic disk of a foreground $> 10^{11} M_\odot$ halo 3% of the time in the Mo et al. (1998) model.

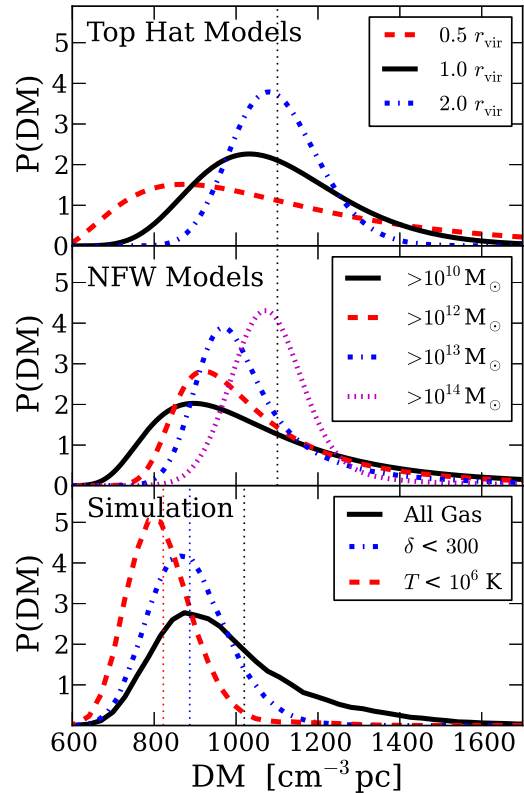


FIG. 2.— $P(\text{DM}|z_s = 1)$ in our analytic models (top two panels) and in the simulation (bottom panel), normalized so that $\int d\text{DM} P(\text{DM}) = 1000$. The different curves illustrate the dependence of this statistic on the extent of the baryonic profile around halos (top panel), on the halo masses that retain their gas (middle), and on baryonic overdensity and temperature thresholds used in the tabulation of DM (bottom). The dotted vertical lines show the mean DM. These lines are slightly offset in the bottom panel owing to star formation in the simulation and/or the specified cuts.

characteristic function is

$$\tilde{P}(t|z_s) = \exp\left(\int_0^{\chi(z_s)} d\chi \left[A + \frac{B^2 \Delta\chi \sigma_p^2}{2}\right]\right), \quad (3)$$

where t is the Fourier dual of DM,

$$A = \int dm_h d^2R a^{-2} n(m_h, z) \left(e^{-it\Delta_{\text{DM}}(R, m_h)} - 1\right),$$

$$B = \int dm_h d^2R a^{-2} n(m_h, z) b(m_h, z) \left(e^{-it\Delta_{\text{DM}}(R, m_h)} - 1\right),$$

R is the proper impact parameter, m_h is the halo mass, Δ_{DM} is a halo's DM profile at R , $n(m_h, z)$ is the comoving number density of halos per m_h , and $b(m_h, z)$ their linear bias. The PDF of DM, $P(\text{DM}|z_s)$, is given by the inverse Fourier transform of $\tilde{P}(t|z_s)$. Equation (3) makes one additional assumption beyond the *standard halo model*, that the value of δ_e for skewers of length $\Delta\chi$ (which has variance σ_p^2) is uncorrelated between adjacent slices. This approximation is accurate for the $\Delta\chi > 100 \text{ Mpc}$ used here. In addition, we trivially generalize equation (3) to include (with the correct linear bias) the diffuse component not associated with halos.

The curves in Figure 2 show $P(\text{DM}|1)$ calculated either using equation (3) or tracing skewers through the simulation. These panels illustrate its dependence on the extent of the gas profile around halos in the top hat models (top panel), on the specified m_* in the NFW profile models (middle panel), and on the properties of the gas used to tabulate DM in the simulations (bottom panel). Generically, all the models predict a high-DM tail to the PDF. This tail is dominated by the most massive systems with $m_h \gtrsim 10^{13} M_\odot$. In addition, the more diffuse the gas around halos or the rarer the halos that can hold onto their gas, the more concentrated is $P(\text{DM}|z_s)$. This trend simply owes to each sightline intersecting a more statistically representative set of structures in the models where the halos' baryonic profiles are more diffuse. Lastly, the core of $P(\text{DM}|1)$ asymptotes to a Gaussian with $\sigma \approx 100 \text{ cm}^{-3} \text{ pc}$ that is determined by large-scale cosmological density correlations in the limit that the baryonic profiles are very diffuse (e.g., $2 r_{\text{vir}}$ case, top panel) or that most sightlines do not intersect a gaseous halo (e.g., $> 10^{14} M_\odot$ case, middle panel).

The simulation allows us to explore how gas at different temperatures and densities contributes to the shape of $P(\text{DM}|z_s)$. The dash-dotted curve in the bottom panel of Figure 2 excludes gas with $\delta_e > 300$ from the tally of DM. The dashed curve excludes gas with $T > 10^6 K$. The comparison of these curves with the solid curve, which includes all of the gas, shows that hot, dense gas (likely associated with $> 10^{12} M_\odot$ halos) contributes to the high-DM tail in the simulations. We have also examined the simulation in Faucher-Giguère et al. (2011) with winds turned off: The high-DM tail essentially disappears in this simulation probably because of overly-efficient star formation.

4. THE DM-GALAXY CROSS CORRELATION

It may not be possible to separate the DM contribution that is intrinsic to the sources from that which is extragalactic. However, this potential difficulty is avoided if sightlines are stacked based on their impact parameters to foreground galaxies. In addition, stacking does not require precise knowledge of the sources' redshifts. Upcoming photometric surveys such as DES and LSST aim to identify most $z \lesssim 1.5$ galaxies over ~ 0.5 of the sky.⁵ Targeted follow-up along each DM sightline is also a possibility. Stacking requires a resolution of $< 0.5'$ (or $\gtrsim 1 \text{ km}$ baselines at 1 GHz) to localize the source to $< 1 r_{\text{vir}}$ of a foreground $z = 0.5, 10^{12} M_\odot$ halo.

The enhancement in DM from a local galaxy with halo mass m_h at impact parameter R is

$$\Delta_{\text{DM}} = \Delta_{1h}(R, m_h) + 2 \int_{r_{\text{min}}}^{\infty} \frac{d\Delta\chi}{a} \zeta_{2h}(\sqrt{\Delta\chi^2 + (R/a)^2}, z),$$

where $\Delta_{1h}(R, m_h)$ is the dispersion measure profile of the halo, $\zeta_{2h} = \rho_e(0) b_h(m_h) \zeta_\delta$, and ζ_δ the 3D matter overdensity correlation function. We calculate the latter, “two halo” term with $r_{\text{min}}/r_{\text{vir}} = 1.5$ and assuming linear theory as in the *standard halo model* (but highly approximate at such small r_{min}).

In a survey with n_{DM} sightlines, the maximum likeli-

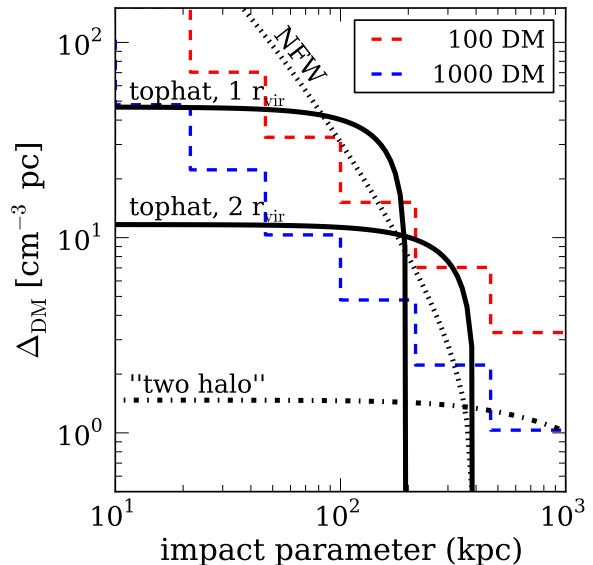


FIG. 3.— Sensitivity to the average DM profile around $m_h \sim 10^{12} M_\odot$ halos of an analysis that stacks sightlines based on their proximity to neighboring galaxies. The solid curves are the DM profile of a $z = 0.5, 10^{12} M_\odot$ halo if the baryons were distributed as a top hat with radius 1 and $2 r_{\text{vir}}$. The dotted curve uses the same specifications except the baryons trace the dark matter with an NFW profile truncated at $2 r_{\text{vir}}$. The dashed piecewise lines are the expected 1σ errors for a survey with 10^2 and 10^3 DM measurements with $z_s \sim 0.5 - 1$, assuming $\overline{\sigma_{\text{DM}}} = 200 \text{ cm}^{-3} \text{ pc}$ and $\ll 1'$ localizations.

hood $\Delta_{\text{DM}}(R, m_h)$ estimator for a Gaussian $P(\text{DM})$ is

$$\hat{\Delta}_{\text{DM}} = \sum_i^{n_{\text{DM}}} \frac{N_i}{\sigma_{\text{DM},i}^2} \left(\widehat{\text{DM}}_i - \overline{\text{DM}} - \delta(z_i) \right) / \sum_i^{n_{\text{DM}}} \frac{N_i}{\sigma_{\text{DM},i}^2} (N_i - \overline{N}_i),$$

where $\overline{Y} = (\sum_i \sigma_{\text{DM},i}^{-2})^{-1} \sum_i Y \times \sigma_{\text{DM},i}^{-2}$ for any variable Y , $\widehat{\text{DM}}_i$ is the estimated DM to source i , N_i is the number of halos along the sightline that fall in the (R, m_h) bin, $\delta(z_i)$ accounts for the change in the background mean $\text{DM}(z_i)$ relative to $\overline{\text{DM}}$ so that $\overline{\delta(z)} = 0$, and $\sigma_{\text{DM},i}^2$ is the variance around the mean $\text{DM}(z_i)$. This estimator assumes that $\delta(z)$ is known, but can easily be generalized to fit a parametric form. The standard deviation of this estimator is

$$\sigma[\hat{\Delta}_{\text{DM}}(R, m_h)] = \sqrt{\frac{\overline{\sigma_{\text{DM}}^2}}{(\overline{N^2} - \overline{N}^2) n_{\text{DM}}}} \approx \sqrt{\frac{\overline{\sigma_{\text{DM}}^2}}{\overline{N} n_{\text{DM}}}}.$$

This error would be reduced if other $\hat{\Delta}_{\text{DM}}(R, m_h)$ bins are estimated simultaneously.

Figure 3 shows the sensitivity of such a stacking analysis to the mean DM profile of $10^{12} M_\odot$ halos. The dashed piecewise lines are the 1σ error for a survey with $n_{\text{DM}} = 10^2$ and 10^3 in a radial bin given by the width of each horizontal line segment. This calculation assumed $\overline{\sigma_{\text{DM}}} = 200 \text{ cm}^{-3} \text{ pc}$ and that each sightline on average intersects two $10^{12} M_\odot$ halos within $1 r_{\text{vir}}$. These numbers roughly approximate our Model 3 for $z_s = 0.5 - 1$ if the intrinsic dispersion in DM is somewhat smaller than the cosmological dispersion (see Figure 1). Figure 3 shows that both the $n_{\text{DM}} = 10^2$ and 10^3 cases are sensi-

⁵ <http://www.darkenergysurvey.org>, <http://www.lsst.org/>

tive to the $1 r_{\text{vir}}$ top hat model – a model that cannot be ruled out with other techniques (Fang et al. 2013) – and the survey with $n_{\text{DM}} = 10^3$ is even sensitive to the $2 r_{\text{vir}}$ model. The sensitivity to $\Delta_{\text{DM}}(R)$ improves [degrades] for a stacking analysis around less [more] massive halos compared to our fiducial $10^{12} M_{\odot}$ case owing to the different \bar{N} . However, this trend is offset (almost perfectly in the top hat models) by the likely increase in Δ_{DM} with halo mass.

5. SCATTERING

Scattering (which broadens an electromagnetic pulse in a frequency-dependent manner owing to path length variations) could result in DM-dependent selection effects. In fact, any millisecond pulse whose sightline intersects an intervening galactic disk is likely to be significantly broadened, over a timescale of

$$\tau_{\text{sc}}^{\text{disk}} = 150 \text{ ms} \times \text{SM}_{-4}^{6/5} \nu_{\text{GHz}}^{-22/5} \quad (4)$$

$$\times \left[\frac{\chi(z)}{1 \text{ Gpc}} \right] \left[1 - \frac{\chi(z)}{\chi(z_s)} \right] (1+z)^{-22/5},$$

where SM_{-4} is the “scattering measure”, in units of $10^{-4} \text{ m}^{-20/3} \text{ kpc}$ (Blandford & Narayan 1985; Cordes & Lazio 2002).⁶ Equation (4) assumed the density power spectrum of Kolmogorov turbulence, as does what follows. For pulsar sightlines above the Milky Way disk plane, $\text{SM}_{-4} \sim 1$, and these sightlines are characteristic of the Milky Way’s thick electron disk (Cordes & Lazio 2002). Thus, $z \lesssim 1$ millisecond transients like those reported in Thornton et al. (2013) whose sightline intersects a gaseous disk similar to the Milky Way are significantly broadened at $\nu_{\text{GHz}} \lesssim 1$. Scattering also impacts the Lovelace & Richards (2013) DM estimation method, erasing correlations between frequencies separated by $\gtrsim (2\pi\tau_{\text{sc}})^{-1}$.

Sightlines passing through a halo’s outskirts are likely to be less broadened by scattering with

$$\tau_{\text{sc}}^{\text{halo}} = 23 \mu\text{s} \times \nu_{\text{GHz}}^{-22/5} \left[\frac{1 \text{ kpc}}{\ell_{\text{out}}} \right]^{4/5} \left(\frac{\mathcal{M}\rho_{e,\text{char}}}{10^{-5} \text{ cm}^{-3}} \right)^{12/5} \quad (5)$$

$$\times \left(\frac{L_{\text{halo}}}{10^2 \text{ kpc}} \right)^{6/5} \left[\frac{\chi(z)}{1 \text{ Gpc}} \right] \left[1 - \frac{\chi(z)}{\chi(z_s)} \right] (1+z)^{-22/5},$$

where ℓ_{out} is the maximum turbulent eddy scale (determined by the driving mechanisms; e.g., infall, winds) and $\mathcal{M}\bar{\rho}_e$ is the standard deviation in the electron number density. For mildly subsonic turbulence, $\rho_{e,\text{char}}$ can roughly be thought of as the characteristic density and \mathcal{M} the typical compressive Mach number (Hopkins 2013). Simulations find $\mathcal{M} \sim 0.1 - 0.2$ at $< 2 r_{\text{vir}}$ for halos with $m_h \sim 10^{15} M_{\odot}$ (Lau et al. 2009), and it is likely that similar Mach numbers apply at lower m_h . For our fiducial parameters – the parameter choices that yield the $23 \mu\text{s}$ coefficient in equation (5) – $\tau_{\text{sc}}^{\text{halo}}$ is larger than the Milky Way contribution of $\tau_{\text{sc}} \sim 0.1 \nu_{\text{GHz}}^{-22/5} \mu\text{s}$ for high-latitude sources (Cordes & Lazio 2002). Moreover, $\tau_{\text{sc}}^{\text{halo}}$ is likely measurable for the Thornton et al. 2013

⁶ We use the latter reference’s expression, which results in 30% larger τ_{sc} , because of the inclusion of non-Gaussianity in the PDF of the deflection angle.

bursts: Setting $\nu = 250 \text{ MHz}$ in equation (5) results in $23 \mu\text{s} \rightarrow 10 \text{ ms}$.

Equation (4) and (5) assumed strong scattering (a requirement for multi-path propagation from a point-source), defined as when the Fresnel scale is larger than the transverse separation at which a ray’s RMS phase differs by π , r_{diff} . In the Milky Way ISM, the ratio of these scales is $f \sim 10^2 \nu_{\text{GHz}}^{-17/10}$ such that strong scattering applies. For the fiducial intrahalo parameters in equation (5), this condition is similarly satisfied with

$$f = 2 \times 10^2 \nu_{\text{GHz}}^{-17/10} a^{11/5} \left(\ell_{\text{out}}^{-2/5} [\mathcal{M}\rho_{e,\text{char}}]^{6/5} L_{\text{halo}}^{3/5} \chi^{1/2} \right)_{\text{fiducial}}.$$

Equation (5) also assumed that the inner scale of turbulence satisfies $\ell_{\text{in}} < r_{\text{diff}} = 1.5 \times 10^{12} \nu_{\text{GHz}}^{6/5} a^{-6/5} \text{ cm}$, much larger than the limit $\ell_{\text{in}} < 10^{10} \text{ cm}$ found in the Milky Way ISM (Armstrong et al. 1995). However, this condition may not be satisfied in the circumgalactic medium. Lithwick & Goldreich (2001) argued that ℓ_{in} is set by the eddy scale at which the turnover time equals the proton diffusion time across the eddy or

$$\ell_{\text{in}} \sim 6 \times 10^{13} \left(\frac{1 \text{ kpc}}{\ell_{\text{out}}} \right)^{1/2} \left(\frac{10^{-4} \text{ cm}^{-3}}{\rho_e/\beta} \right)^{3/2} \text{ cm}, \quad (6)$$

where β is the plasma beta parameter (the ratio of thermal to magnetic pressure) which is likely > 1 in the intrahalo medium. However, it is also possible that the inner scale is set by the much smaller proton-gyro radius (Schekochihin et al. 2009).⁷ If $r_{\text{diff}} < \ell_{\text{in}}$, $\tau_{\text{sc}}^{\text{halo}}$ would be reduced by the factor $\sim (r_{\text{diff}}/\ell_{\text{in}})^{1/3}$ as long as the scattering remained strong.

Pulse broadening with the expected frequency dependence for scattering was detected in one of the four bursts reported in Thornton et al. (2013), for which Lorimer et al. (2013) estimated $\hat{\tau}_{\text{sc}} = 3.7 \text{ ms}$ at 1 GHz . In addition, $\hat{\tau}_{\text{sc}} = 20 \text{ ms}$ was found for the Lorimer et al. (2007) burst. These $\hat{\tau}_{\text{sc}}$ both suggest that either (1) the scattering is intrinsic to the source or (2) the sightline intersected a galactic disk. However, the latter seems unlikely unless electronic disks have significantly larger radii than we have estimated (see footnote 4).

6. CONCLUSIONS

We showed that the standard deviation around the mean $\text{DM}(z)$ is $100 - 400 \text{ cm}^{-3} \text{ pc}$ at $z = 0.5 - 1$, with its exact value being sensitive to how the baryons are distributed in the outskirts of dark matter halos. Extragalactic DM measurements could constrain the locations of the cosmic baryons either by directly measuring the probability distribution of the intergalactic DM or by stacking based on the separation to field galaxies. The former method requires both the sources’ redshifts as well as knowledge of their intrinsic $\sigma[\text{DM}]$ to a precision of $\ll 400 \text{ cm}^{-3} \text{ pc}$, whereas the latter requires sub-arcminute localization and the identification of coincident galaxies.

⁷ In $\beta \gg 1$ Alfvénic turbulence it is likely that density fluctuations are suppressed relative to velocity fluctuations by the factor β , likely resulting in smaller $\tau_{\text{sc}}^{\text{halo}}$ than predicted by equation (5).

We thank Chris Hirata, Ryan O’Leary, Eliot Quataert, Martin White, and Jennifer Yeh for helpful conversations, and Claude-André Faucher-Giguère for sharing the

simulations used in this work. MM acknowledges support by the National Aeronautics and Space Administration through the Hubble Postdoctoral Fellowship.

REFERENCES

- Armstrong, J. W., Rickett, B. J., & Spangler, S. R. 1995, *ApJ*, 443, 209
- Behroozi, P. S., Wechsler, R. H., & Conroy, C. 2013, *ApJ*, 770, 57
- Blandford, R., & Narayan, R. 1985, *MNRAS*, 213, 591
- Bregman, J. N. 2007, *Ann. Rev. Astron. & Astrophys.*, 45, 221
- Bullock, J. S., Kolatt, T. S., Sigad, Y., Somerville, R. S., Kravtsov, A. V., Klypin, A. A., Primack, J. R., & Dekel, A. 2001, *MNRAS*, 321, 559
- Cen, R., & Ostriker, J. P. 1999, *ApJ*, 514, 1
- Cooray, A., & Sheth, R. 2002, *physrep*, 372, 1
- Cordes, J. M., & Lazio, T. J. W. 2002, *arXiv:astro-ph/0207156*
- Dai, X., Bregman, J. N., Kochanek, C. S., & Rasia, E. 2010, *ApJ*, 719, 119
- Fang, T., Bullock, J., & Boylan-Kolchin, M. 2013, *ApJ*, 762, 20
- Faucher-Giguère, C.-A., Kereš, D., & Ma, C.-P. 2011, *MNRAS*, 417, 2982
- Fukugita, M., & Peebles, P. J. E. 2004, *ApJ*, 616, 643
- Hopkins, P. F. 2013, *MNRAS*, 430, 1880
- Inoue, S. 2004, *MNRAS*, 348, 999
- Ioka, K. 2003, *ApJL*, 598, L79
- Kauffmann, G., et al. 2003, *MNRAS*, 341, 33
- Lau, E. T., Kravtsov, A. V., & Nagai, D. 2009, *ApJ*, 705, 1129
- Lieu, R., & Duan, L. 2013, *ApJL*, 763, L44
- Lithwick, Y., & Goldreich, P. 2001, *ApJ*, 562, 279
- Lorimer, D. R., Bailes, M., McLaughlin, M. A., Narkevic, D. J., & Crawford, F. 2007, *Science*, 318, 777
- Lorimer, D. R., Karastergiou, A., McLaughlin, M. A., & Johnston, S. 2013, *ArXiv:1307.1200*
- Lovelace, R. V. E., & Richards, D. W. 2013, *MNRAS*, 433, 2275
- Mo, H. J., Mao, S., & White, S. D. M. 1998, *MNRAS*, 295, 319
- Navarro, J. F., Frenk, C. S., & White, S. D. M. 1996, *ApJ*, 462, 563
- Penton, S. V., Stocke, J. T., & Shull, J. M. 2004, *ApJS*, 152, 29
- Planck Collaboration, et al. 2013, *ArXiv:1303.5076*
- Schekochihin, A. A., Cowley, S. C., Dorland, W., Hammett, G. W., Howes, G. G., Quataert, E., & Tatsuno, T. 2009, *ApJS*, 182, 310
- Sharma, P., McCourt, M., Quataert, E., & Parrish, I. J. 2012, *MNRAS*, 420, 3174
- Sheth, R. K., & Tormen, G. 2002, *MNRAS*, 329, 61
- Shull, J. M., Smith, B. D., & Danforth, C. W. 2012, *ApJ*, 759, 23
- Springel, V. 2005, *MNRAS*, 364, 1105
- Springel, V., & Hernquist, L. 2003, *MNRAS*, 339, 312
- Thornton, D., et al. 2013, *Science*, 341, 53
- Wolfe, A. M., Gawiser, E., & Prochaska, J. X. 2005, *Ann. Rev. Astron. & Astrophys.*, 43, 861
- Zhang, P., & Sheth, R. K. 2007, *ApJ*, 671, 14